frontiers | Frontiers in Energy Research

TYPE Original Research
PUBLISHED 29 September 2022
DOI 10.3389/fenrg.2022.1005796

OPEN ACCESS

EDITED BY
Liansong Xiong,
Nanjing Institute of Technology (NJIT), China

REVIEWED BY
Tingting Sun,
Hefei University of Technology, China
Bowen Wang,
Kashgar University, China
Zongbo Li,
Xi'an Jiaotong University, China

*CORRESPONDENCE
Jiangdong Cao,
caojd@jssc.edu.cn

SPECIALTY SECTION
This article was submitted to Process and Energy Systems Engineering, a section of the journal Frontiers in Energy Research

RECEIVED 28 July 2022
ACCEPTED 22 August 2022
PUBLISHED 29 September 2022

CITATION
You J, Xu D and Cao J (2022), Dynamic power-based temporary frequency support scheme for a wind farm. *Front. Energy Res.* 10:1005796. doi: 10.3389/fenrg.2022.1005796

Dynamic power-based temporary frequency support scheme for a wind farm

Jiahan You, Dan Xu and Jiangdong Cao*

School of Intelligent Manufacturing and Information, Jiangsu Shipping College, Nantong, China

Doubly fed induction generators can participate in frequency support following a disturbance by releasing their rotational energies. However, when regaining the rotor speed, a secondary frequency dip (SFD) tends to produce a sudden output drop. This study suggests a dynamic power-based stepwise inertial control (IC) scheme of a wind power plant for minimizing the SFD while reducing the maximum frequency deviation (MFD), considering the non-negligible wake. To this end, the reference of the output power increases to the torque limit. Afterward, the power reference smoothly decays with the dynamically decreasing incremental power and then automatically switches to the maximum power point tracking operation. The performance of the temporary frequency support with the suggested stepwise IC strategy is investigated with various penetration levels of wind power. Test results demonstrate that the suggested stepwise IC strategy can minimize the SFD and reduce mechanical stresses on the wind turbine during the recovery of the rotor speed while reducing the MFD. Therefore, the suggested stepwise IC strategy secures the dynamic frequency stability of an electric power system dominated by wind power generations.

KEYWORDS

stepwise inertial control, power system control, second frequency dip, mechanical stress, rotor speed recovery

Introduction

The electric power system faces challenges of system frequency stability with high-wind-power-penetrated power girds (Wang et al., 2020). The reasons for this phenomenon are explained as follows: doubly fed induction generators (DFIGs) are unable to sustain the system frequency since they decouple the speed of the rotor from the frequency (Xiong et al., 2020; Guo et al., 2022). This results in a reduction in the system inertia response and primary frequency response (Gevorgian et al., 2015; Yang et al., 2021). The range of operation of the DFIG is almost six times that of the conventional synchronous generators (SGs) due to the various characteristics of the DFIG and SG; therefore, the DFIG can be a strong choice to sustain the system frequency (Wang and Tomsovic, 2018). Thus, DFIGs are required to participate in inertial control (IC) to preserve the frequency stability of the power grid.

The IC strategies can be roughly divided into three classifications characterized by the definition of the shape of the power reference: *df/dt*-based IC, frequency deviation-based IC, and stepwise IC (Morren et al., 2006; Vyver et al., 2016; Li et al.,2017; Hu and WU, 2019; Wu et al., 2019; Kheshti et al., 2019; Peng et al., 2020). The *df/dt*-based IC can emulate the inertia response to support the reduced inertia response. Frequency deviation-based IC is capable of emulating the primary frequency response to reduce the maximum grid frequency deviation (MGFD). A stepwise IC scheme is determined by the preset power reference trajectories and not the measured grid frequency. The power reference trajectories can be a temporary frequency control trajectory (Yang et al., 2018) and a reliable power reference trajectory (Kheshti et al., 2019). The stepwise IC can boost the grid frequency at a high level owing to the rapid frequency support response (Yang et al., 2018; Kheshti et al., 2019). However, after performing the frequency support response, the rotor speed is required to be regained up to the optimal speed, such a process tends to cause a second frequency drop (SFD) (Lao et al., 2020).

A constant stepwise power reference is addressed to regain the rotor speed (Ullah et al., 2008), and due to the sudden output power drop, an SFD is inevitable. To mitigate the SFD, the authors (Hafiz and Abdennour, 2015) suggest that the power reference of the wind turbines decays in a ramp manner during the recovery period of the rotor speed. The authors (Kang et al., 2016; Xu and Xu, 2017) propose a fixed power reference scheme and a constantly accelerating power reference based on mechanical power to regain the rotor speed, however, the SFD still exists due to the sudden power reduction; furthermore, the output power reduction to counterbalance the SFD and the rotor speed recovery is difficult to determine. A two-level variable coefficient-based controller is designed for DFIG (Xiong et al., 2021). However, the effectiveness of the two-level scheme strongly depends on the predetermined training of the fuzzy controller.

This study addresses a dynamic power-based stepwise IC strategy of the wind power plant with the purpose of minimizing the SFD and mechanical stresses on the wind turbine during the recovery of the rotor speed while reducing the MGFD. To this end, the power reference increases to the torque limit. Afterward, the power reference smoothly decays with the dynamically decreasing incremental power and then automatically switches to the maximum power point tracking operation (MPPTO). The benefits of the proposed stepwise IC strategy are indicated with various penetration levels of wind power.

Doubly fed induction generator model

The mechanical power captured from the wind through the wind turbine can be defined as a nonlinear function of the rotor radius (R), air density (ρ), wind speed (vw), pitch angle (β), tip-speed ratio (λ), and power coefficient (c_p), as follows:

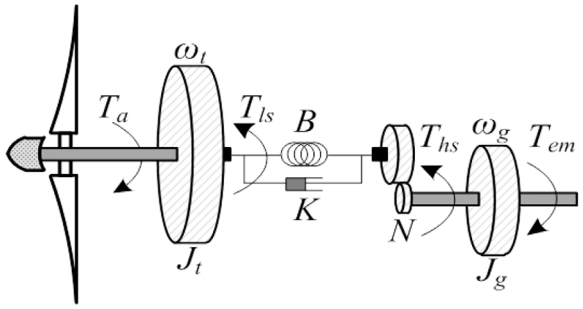

FIGURE 1
Two-mass model.

$$P_m = \frac{1}{2}\rho\pi R^2 v_{wind}^3 c_P(\lambda,\beta), \tag{1}$$

$$c_P(\lambda,\beta) = 0.645\left\{0.00912\lambda + \frac{-5 - 0.4(2.5+\beta) + 116\lambda_i}{e^{21\lambda_i}}\right\}, \tag{2}$$

$$\lambda_i = \frac{1}{\lambda + 0.08(2.5+\beta)} - \frac{0.035}{1 + (2.5+\beta)^3}, \tag{3}$$

$$\lambda = \frac{\omega_r R}{v_w}. \tag{4}$$

In (1), c_p has a maximum value ($c_{P,\,\max}$) at the optimal tip-speed ratio (λ_{opt}), where the DFIG can capture the maximum power from the wind. The formula of the MPPTO is as follows:

$$P_{MPPT} = \frac{1}{2}\rho\pi R^2\left(\frac{\omega_r R}{\lambda_{opt}}\right)^3 c_{P,\max} = k_g\omega_r^3, \tag{5}$$

where P_{MPPT} is the reference for the MPPTO and k_g is set to 0.512.

To model the mechanical dynamics, a two-mass shaft model, which is expressed in (6)–(8), is employed in this study (see Figure 1). T_{wt}, H_t, ω_t, T_m, H_g, and ω_r are the mechanical torques, inertia constants, and rotor speeds of the turbine and generator, respectively. T_e is the generator's electrical torque. K and B are the spring constant and damping constant, respectively. θ_t and θ_{ls} are the displacements of the angular of the turbine rotor and low-speed shaft, respectively. ω_{ls} is the low-speed shaft rotor speed, as shown in (Boukhezzar and Siguerdidjane, 2011).

$$2H_t\frac{d\omega_t}{dt} = T_m - T_{ls}, \tag{6}$$

$$2H_g\frac{d\omega_r}{dt} = T_{hs} - T_{em}, \tag{7}$$

$$T_{ls} = K(\theta_t - \theta_{ls}) + B(\omega_t - \omega_{ls}). \tag{8}$$

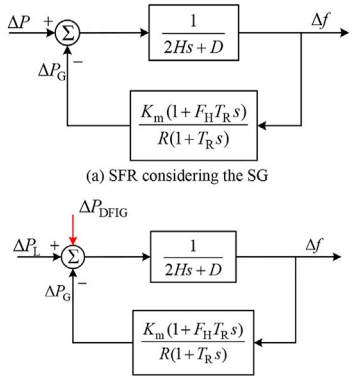

FIGURE 2
SFR of the single machine model.

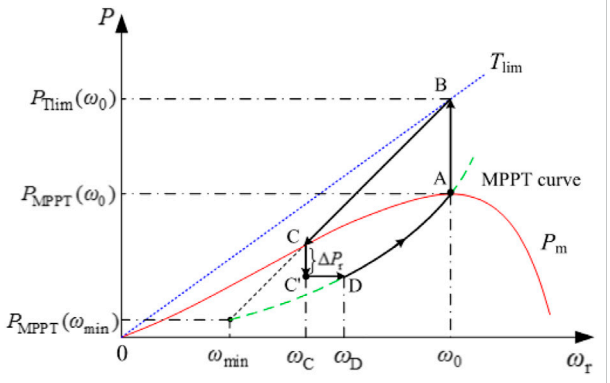

FIGURE 3
Operational concepts of the conventional stepwise IC scheme.

Stepwise inertial control of a wind power plant

During the frequency support phase (FSP), active power is injected into the grid by decreasing the rotor speed. When designing the stepwise IC scheme, more attention should be paid to the stalling of the rotor speed. During the rotor speed recovery phase (RSRP), the rotor speed is restored by absorbing the power from the grid; the degree of the SFD should be noticed when designing the control strategy.

As illustrated in Figure 2A, based on the low-order system frequency response model (shi et al., 2018), the system frequency deviation ($\Delta f\ (t)$) in the time domain can be represented as follows:

$$\Delta f\,(t) = \frac{\Delta P}{K_1 + D}\left[1 + \alpha e^{-\xi\omega_n t}\sin\left(\omega_d t + \beta\right)\right], \tag{9}$$

$$\omega_n = \sqrt{\frac{DR + K_m}{2HRT_R}}, \tag{10}$$

$$\xi = \left(\frac{2HR + (DR + K_m F_H)T_R}{2\,(DR + Km)}\right)\omega_n, \tag{11}$$

where ω_n, ξ, and ω_d are the natural oscillation frequency, damping ratio, and damped frequency, respectively. α and β are the derived coefficients from the SFR model. ΔP is the size of the disturbance.

The maximum frequency deviation and frequency nadir can be given as shown in Eqs 14 and 15, respectively, by deriving the occurrence time of the frequency nadir.

$$\Delta f_{\max} = \frac{\Delta P}{K_1 + D}\left(1 + \alpha_1 e^{-\xi\omega_n t_{nadir}}\right), \tag{12}$$

$$f_{nadir} = f_{nom} - \Delta f_{\max} = f_{nom} - \frac{\Delta P}{K_1 + D}\left(1 + \alpha_1 e^{-\xi\omega_n t_{nadir}}\right), \tag{13}$$

where K_1 is the setting value of the primary governor response. f_{nom}, $\Delta f_{\max}$, and f_{nadir} are the nominal system frequency, maximum frequency deviation, and frequency nadir, respectively.

As shown in (Yang et al., 2022), the improved SFR model is represented as shown in Figure 2B. The equivalent size of disturbance (ΔP) is calculated as follows:

$$\Delta P = \Delta P_L - \Delta P_{DFIG}, \tag{14}$$

where ΔP_{DFIG} indicates the additional power from the DFIG when performing temporary frequency support.

Thus, frequency nadir can be rearranged as follows:

$$f_{nadir} = f_{nom} - \frac{\Delta P_L - \Delta P_{DFIG}}{K_1 + D}\left(1 + \alpha_1 e^{-\xi\omega_n t_{nadir}}\right). \tag{15}$$

In (Eq. 15), it is evidenced that the DFIG supports system frequency after the system frequency changes. The instantaneous system frequency is higher, thereby reducing the maximum system frequency deviation with the larger ΔP_{DFIG}. Furthermore, in the RSRP, if a larger ΔP_{DFIG} instantly decreases from the power reference, a severe SFD tends to be produced. If ΔP_{DFIG} smoothly decreases, the depth of the SFD can be reduced.

Conventional stepwise inertial control scheme

Figure 3 displays the features of the conventional stepwise IC scheme, which includes two sequential stages highlighted in the black line: FSP (line A to C) and RSRP (line C to D). Prior to a severe disturbance, the DFIG operates in the MPPTO, which corresponds

to point A. Upon detecting a disturbance, to reduce $\Delta f_{\max}$, the DFIG instantly increases its output power from P_0 to $P_{T\lim}(\omega_0)$, which is the torque limit at ω_0 and corresponds to point B, as shown in Figure 3. To avoid the stalling of the rotor speed, the power reference for stepwise IC (P_{set}) is defined as follows:

$$P_{set} = \frac{P_{T\lim}(\omega_0) - P_{MPPT}(\omega_{\min})}{\omega_0 - \omega_{\min}}(\omega_r - \omega_{\min}) + P_{MPPT}(\omega_{\min}), \tag{16}$$

where $P_{\mathrm{MPPT}}(\omega_0)$ is the power reference of the MPPT operation prior to a disturbance. $\omega_{\min}$ is the minimum rotor speed. $P_{MPPT}(\omega_{\min})$ is the value of P_{MPPT} at $\omega_{\min}$.

A conventional stepwise IC scheme can reduce the MFD since a certain amount of kinetic energy is rapidly released in the early stage of a frequency disturbance. The released kinetic energy (ΔE) during the FSP can be expressed as follows:

$$\Delta E = 0.5 J_{DFIG}(\omega_0^2 - \omega_C^2), \tag{17}$$

where J_{DFIG} represents the moment of inertia of the DFIG. ω_C is the rotor speed at operating point C, as shown in Figure 3.

According to the swing equation, since the output power of the DFIG is more than P_m, the rotor speed decreases so that P_{set} decreases with ω_r from operating point B to operating point C. It should be noticed that ω_r would converge to point C, which indicates the intersection of the P_m curve and (16). Thus, the conventional stepwise IC strategy avoids stalling of ω_r since ω_C is located in the stable operating region.

After ω_r convergence, the conventional stepwise IC scheme instantly reduces the reference of the output power from $P_{set}(\omega_C)$ to $P_{set}(\omega_C) - \Delta P_r$, so as to restore ω_r, and then, is kept until P_{set} meets the MPPTO curve. At point D, P_{ref} is changed back to P_{MPPT}, as shown in Eq. 5, and then, ω_r is restored to ω_0. The power reference for lines C to A can be expressed as shown in Eqs 18 and 19. It should be noted that to reduce the depth of the SFD, a small ΔP_r is inevitable; nevertheless, the rotor speed recovery is extended, and vice versa.

$$P_{\mathrm{set}} = P_{\mathrm{set}}(\omega_{\mathrm{C}}) - \Delta P_{\mathrm{r}}, \tag{18}$$

$$P_{\mathrm{set}}(\omega_{\mathrm{r}}) = P_{\mathrm{MPPT}}(\omega_{\mathrm{r}}). \tag{19}$$

To recover the rotor speed at point C, as shown in Figure 3, the swing equations on the DFIG and power system can be expressed as follows:

$$2H_{DFIG}\omega_r \frac{d\omega_r}{dt} = \Delta P_{\mathrm{r}}, \tag{20}$$

$$2Hf_{\mathrm{sys}} \frac{df_{\mathrm{sys}}}{dt} = (\Delta P_G - \Delta P_L - \Delta P_{\mathrm{r}}), \tag{21}$$

where H_{DFIG} is the inertial time constant of the DFIG.

As shown in Eqs 20 and 21, ΔP_r with rapid variation characteristics causes a subsequent disturbance to the power grid, which leads to an SFD; furthermore, the size of the SFD is dependent on ΔP_r. Figure 4 illustrates the results of the conventional stepwise IC strategy with different settings for ΔP_r. As shown in (20), with a large ΔP_r, the rotor speed recovery is rapid and a severe SFD is produced (as seen in Eq. 21).

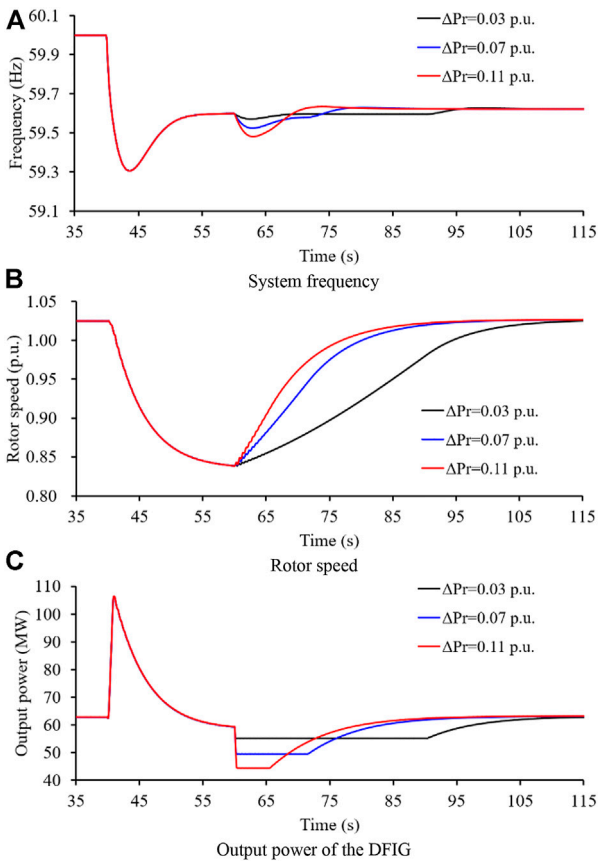

FIGURE 4
Results of the conventional scheme with various forms of ΔP_r.

Implementation of the conventional scheme may face several challenges, which are as follows: 1) The tradeoff between the depth of the SFD and rotor speed recovery is difficult to achieve. 2) The control strategy of the conventional RSR scheme may cause instability issues if a sudden disturbance occurs.

Proposed stepwise inertial control scheme

To address the abovementioned issues of the conventional stepwise IC scheme, this study suggests a dynamic power-based stepwise IC of a DFIG, which combines the FSP and RSRP, as shown in Figure 5.

When the system frequency exceeds the deadband, the DFIG starts up the stepwise IC controller. The power reference for stepwise IC is illustrated as follows:

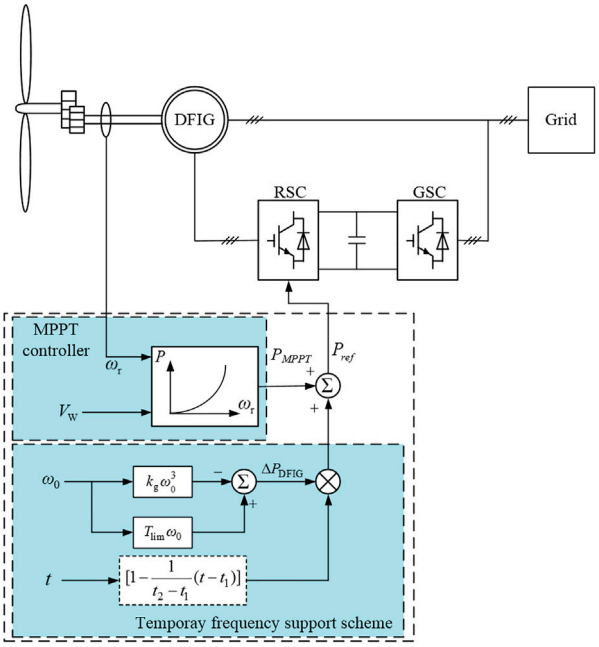

FIGURE 5
Control concept of dynamic power-stepwise IC scheme.

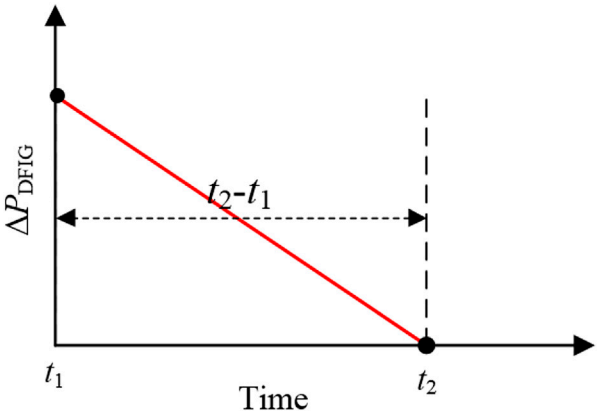

FIGURE 6
Regulation characteristics of ΔP_{DFIG}.

$$P_{ref}(\omega_r, t) = P_{MPPT} + \Delta P_{DFIG}, \tag{22}$$

$$\Delta P_{DFIG} = [P_{\mathrm{Tlim}}(\omega_0) - P_{\mathrm{MPPT}}(\omega_0)] \times \left[1 - \frac{1}{t_2 - t_1}(t - t_1)\right], \tag{23}$$

where ΔP_{DFIG} is the incremental power. t_1 is the instant of the initiation of the stepwise IC scheme. t_2 indicates the instant for

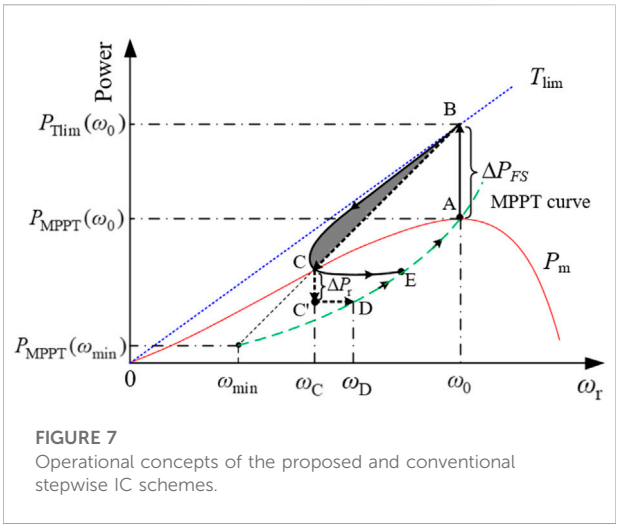

FIGURE 7
Operational concepts of the proposed and conventional stepwise IC schemes.

meeting the MPPTO curve, and thus, t_2–t_1 represents the scheduled time for decreasing the ΔP_{DFIG} to 0.

As illustrated in (Eq. 23) and Figure 6, it is evidenced that smaller t_2–t_1 is able to accelerate the rotor speed restoration, but a severe SFD tends to follow the sudden output drop. Hence, t_2–t_1 should be not set as too small a value. The large enough t_2–t_1 can avoid the risk of the SFD but considerably delays the rotor speed restoration. Normally, the rotor speed should be regained before the initiation of the secondary frequency drop. Thus, t_2–t_1 is set as 10.0–30.0s for different power systems considering the response time of secondary frequency response of the power system.

As shown in Figure 7, similar to the conventional stepwise IC scheme, at t_0, the power reference increases to $P_{\mathrm{Tlim}}(\omega_0)$ corresponding to the operating point A to point B. Afterward, different from the conventional stepwise IC, the incremental power smoothly decreases based on the linear function. Thus, the power reference smoothly decays and automatically switches to the MPPTO curve corresponding to the operating point B to operating point A through operating points C and E.

As illustrated in Figure 7 ($\omega_0 \rightarrow \omega_C$ phase), since the solid segment BC is higher than the dotted segment BC, more power is released to the electric grid in the initial stage of a disturbance with the same energy release; as a result, the MFD of the proposed stepwise IC strategy is reduced while ω_r is regained earlier than the conventional stepwise IC scheme. The reasons for the solid segment BC being higher than the dotted segment BC are explained as follows.

The derivative functions of Eqs 16 and 20 are represented as follows:

$$\frac{dP_{\mathrm{set}}}{d\omega_r} = \frac{P_{\mathrm{Tlim}}(\omega_0) - P_{\mathrm{MPPT}}(\omega_{\mathrm{min}})}{\omega_0 - \omega_{\mathrm{min}}}, \tag{24}$$

$$\frac{dP_{\mathrm{ref}}}{d\omega_r} = \frac{dP_{\mathrm{MPPT}}(\omega_r)}{d\omega_r} = 3k_g\omega_r^2. \tag{25}$$

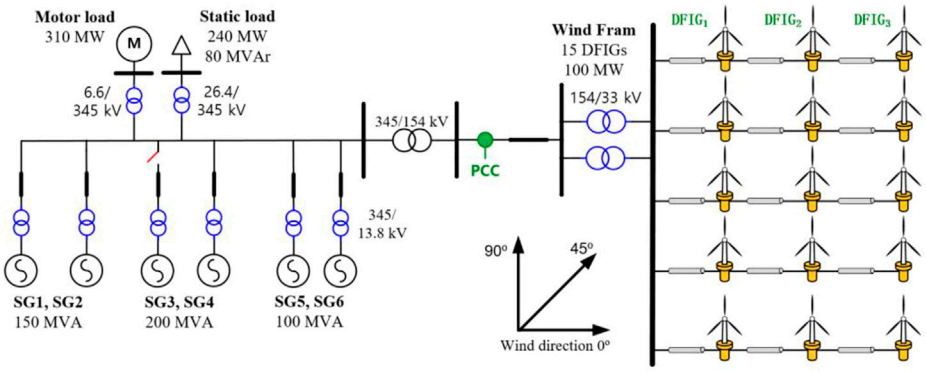

FIGURE 8
Test system.

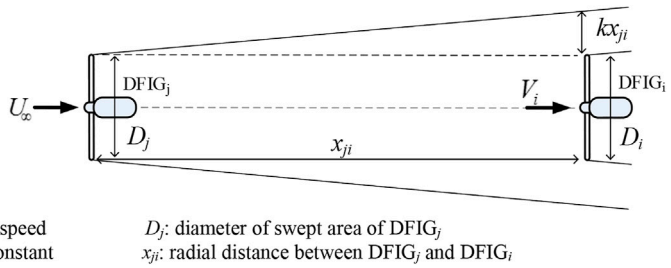

U_∞: incoming wind speed
k: wake-decaying constant
D_j: diameter of swept area of DFIG$_j$
x_{ji}: radial distance between DFIG$_j$ and DFIG$_i$

FIGURE 9
Shadow cone.

As shown in Eq. 24, $dP\text{set}/dt$ decreases with the increasing ω_r and is fixed at a constant wind speed condition. Comparing (24) and (25), with $\omega_0 \leq 1.12$ p. u. and $dP_{set}/d\omega_0 \geq dP_{ref}/d\omega_r$, as a result, the solid segment BC is higher than the dotted segment BC.

In addition, compared with the conventional fixed power-based rotor speed recovery scheme, the output power of the proposed stepwise IC scheme smoothly decreases and automatically switches to the MPPTO curve through the dynamic power reference suggested, as shown in Eq. 22. This process corresponds to the solid segment CE, as shown in Figure 7. Therefore, the smooth decreasing power is a benefit to reducing/removing the second drop on the system frequency and further reducing mechanical stresses on the shaft of the DFIG.

Model system and simulations

Simulations on various penetration levels of wind power are conducted to explore the performance of the proposed stepwise IC strategy. The model system shown in Figure 8, which comprises a wind farm and six steam turbine SGs, is employed. The droop coefficient for all conventional SGs is set to 5.0%. The deadband of the governor response for all synchronous generators is set to 33 mHz. IEEEX1 is used for voltage control of conventional SGs.

For calculating the wind speeds of the DFIGs in a wind power plant, the Park wake model, which is based on the Jenson model, is implemented, as illustrated in Figure 9. The wake wind speeds of the DFIGs are derived since the wind direction and cumulative impact of multiple shadowing are considered (Koch et al., 2005). The wind speed of a DFIG$_i$ and V_i can be calculated as follows:

$$V_i = U_\infty \left[1 - 2\sqrt{\sum_{\substack{j=1 \\ j \neq i}}^{n} \left\{ a_j \left(\frac{D_j}{D_i + 2kx_{ji}} \right)^2 \beta_{ji} \right\}^2}\right], \quad (26)$$

where β_{ji} indicates the ratio between the swept and overlapping areas of the DFIG$_i$, a_j is the factor of the axial induction of the DFIG$_j$, and n is the number of DFIGs in a wind farm.

TABLE 1 Parameters of the DFIG.

Item	Value	Unit
Apparent power	5.5	MVA
Active power	5.0	MW
Stator voltage	2.3	kV
Stator resistance	0.023	p.u
Stator leakage reactance	0.18	p.u
Magnetizing reactance	2.9	p.u
Rotor resistance	0.016	p.u
Rotor leakage reactance	0.16	p.u
Stable operating range of ω_r	0.70–1.25	p.u
Rated, cut-in, and cut-out speeds	11, 4, and 25	m/s

The wind speeds for the $DFIG_1$, $DFIG_2$, and $DFIG_3$ are 9.0 m/s, 8.4 m/s, and 7.8 m/s, respectively. The available rotor kinetic energies are 3.92, 1.89, and 1.66s, respectively. The parameters of the DFIG are shown in Table 1. To provide clear explanations of the proposed scheme, there are two settings for the proposed and conventional stepwise IC schemes. This first setting is that Δt of the proposed stepwise IC scheme for the first column DFIGs ($DFIG_1$), second column DFIGs ($DFIG_2$), and third column DFIGs ($DFIG_3$) are set as 28.5, 17.0, and 11.0s to achieve the same energy release with the conventional scheme; the second setting is that ΔP_r for all DFIGs are set as 0.05 p. u., which is referred in the Technical standards GB, (2018) and 0.10 p. u., respectively.

As a disturbance, the SG_3, which generates 120 MW, is tripped out. Furthermore, the wind penetration level of case 1 and case 2 are 13.6 and 27.3%, respectively. The performance of the proposed stepwise IC strategy is compared to those of the MPPTO and conventional stepwise IC strategy with respect to reducing the MFD, nadir-based frequency response (NBFR), second frequency nadir, and mechanical stresses.

Case 1: wind penetration level of 13.6%

As shown in Figure 10A, the MFD of the MPPTO is 1.222 Hz, which is higher than that of the conventional stepwise IC method by 0.240 Hz, since more kinetic energy is released for the conventional method while no kinetic energy is released for the MPPTO, as shown in Figure 10B. The MFD for the proposed stepwise IC method is 0.964 Hz, which is less than that of the conventional stepwise IC method by 0.018 Hz, even though the same rotor energy is released from DFGs as in the conventional stepwise IC schemes. The reason for this performance is that the injected power is more than that in the conventional stepwise IC method in the initial period of the disturbance (as seen in Figure 10B). The NBFR with the suggested stepwise IC method is 124.48 MW/Hz; however, NBFRs with the conventional stepwise IC method and MPPTO are 122.20 MW/Hz and 98.20 MW/Hz, respectively, as shown in Table 1, due to the higher frequency nadir in the proposed stepwise IC method.

As shown in Figures 10C, F, and I, the output powers of the conventional stepwise IC scheme suddenly decrease at different instants so that the system frequency drops again. As shown in Figure 10A, the depth of the SFD of the conventional stepwise IC scheme with large ΔP_r is less severe than the conventional stepwise IC scheme with small ΔP_r. However, the output powers of the $DFIG_1$, $DFIG_2$, and $DFIG_3$ smoothly decay over time until the reference of the output power switches to the MPPTO curve. This is the reason that the suggested stepwise IC scheme can reduce the depth of the SFD. In addition, since the suggested stepwise IC scheme can regulate the time for meeting the MPPTO curve without the requirement of mechanical power, it can ensure the rapid recovery of the rotor speed and system frequency stabilization, as illustrated in Figure 10.

As shown in Figures 10E, H, and K, for the conventional stepwise IC schemes and proposed stepwise IC scheme, mechanical stresses on the wind turbines are caused due to the rapid power increase flow of the disturbance. Such phenomena are inevitable while improving the frequency nadir. However, mechanical stresses of the wind turbines for the conventional stepwise IC schemes are caused due to the rapid power reduction and mechanical stresses become severe with the increasing ΔP_r. However, the proposed stepwise IC scheme can avoid mechanical stresses on the wind turbine in the RSRP since the incremental power smoothly decreases to zero, as shown in Figure 10L.

Case 2: wind penetration level of 27.3%

To realize a high wind penetration of 27.3%, SG_5 is out of service and the capacity of the wind power plant increases to 150 MW. Thus, the inertial response and primary frequency response of the power system become worse.

As illustrated in Figure 11, the frequency nadir and NBFR with the MPPTO are 58.619 Hz and 86.98 MW/Hz, respectively, which are lower than those of case 1 due to the increased wind power penetration. However, frequency nadirs and NBFRs for the conventional and proposed stepwise IC schemes become better than those in case 1 since the power output of wind power in MW is more than that in case 1. In addition, the improvements of the frequency nadir and NBFR for the suggested stepwise IC scheme are more than that in the conventional stepwise IC schemes.

Output powers of the conventional stepwise IC scheme suddenly decrease at different instants so that the system frequency drops again. As shown in Figure 11A, the depth of the SFD of the conventional stepwise IC scheme with large ΔP_r is less severe than the conventional stepwise IC scheme with small ΔP_r. In addition, mechanical stresses of the wind turbines are created owing to the rapid power reduction. However, the output powers of the $DFIG_1$, $DFIG_2$, and $DFIG_3$ smoothly decay over time until the reference of the output power switches to the MPPTO curve. This is the reason that the suggested stepwise IC scheme can reduce the depth of the SFD and reduce the mechanical stresses of the DFIGs.

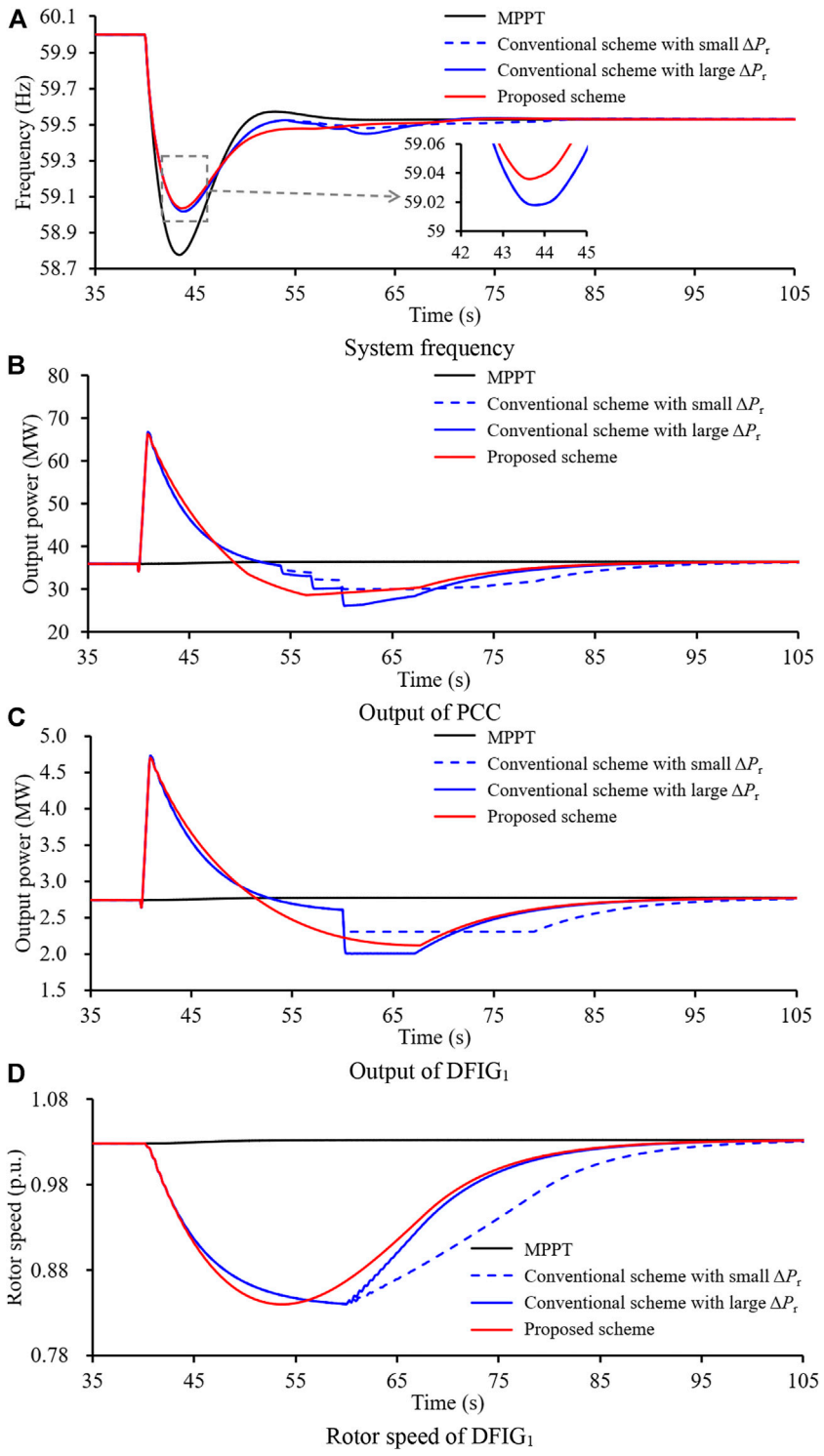

FIGURE 10
Results for case 1.

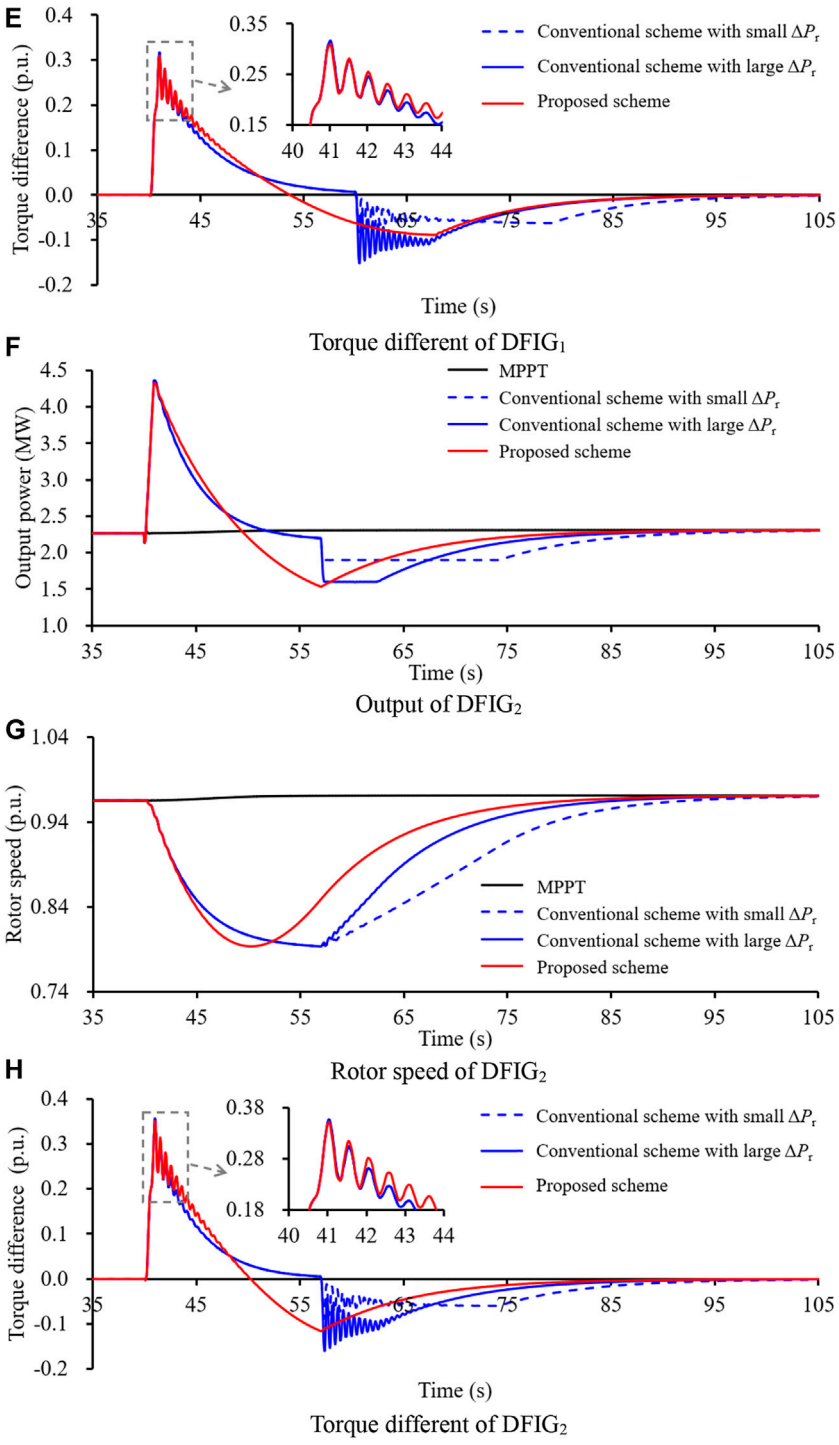

FIGURE 10
continued.

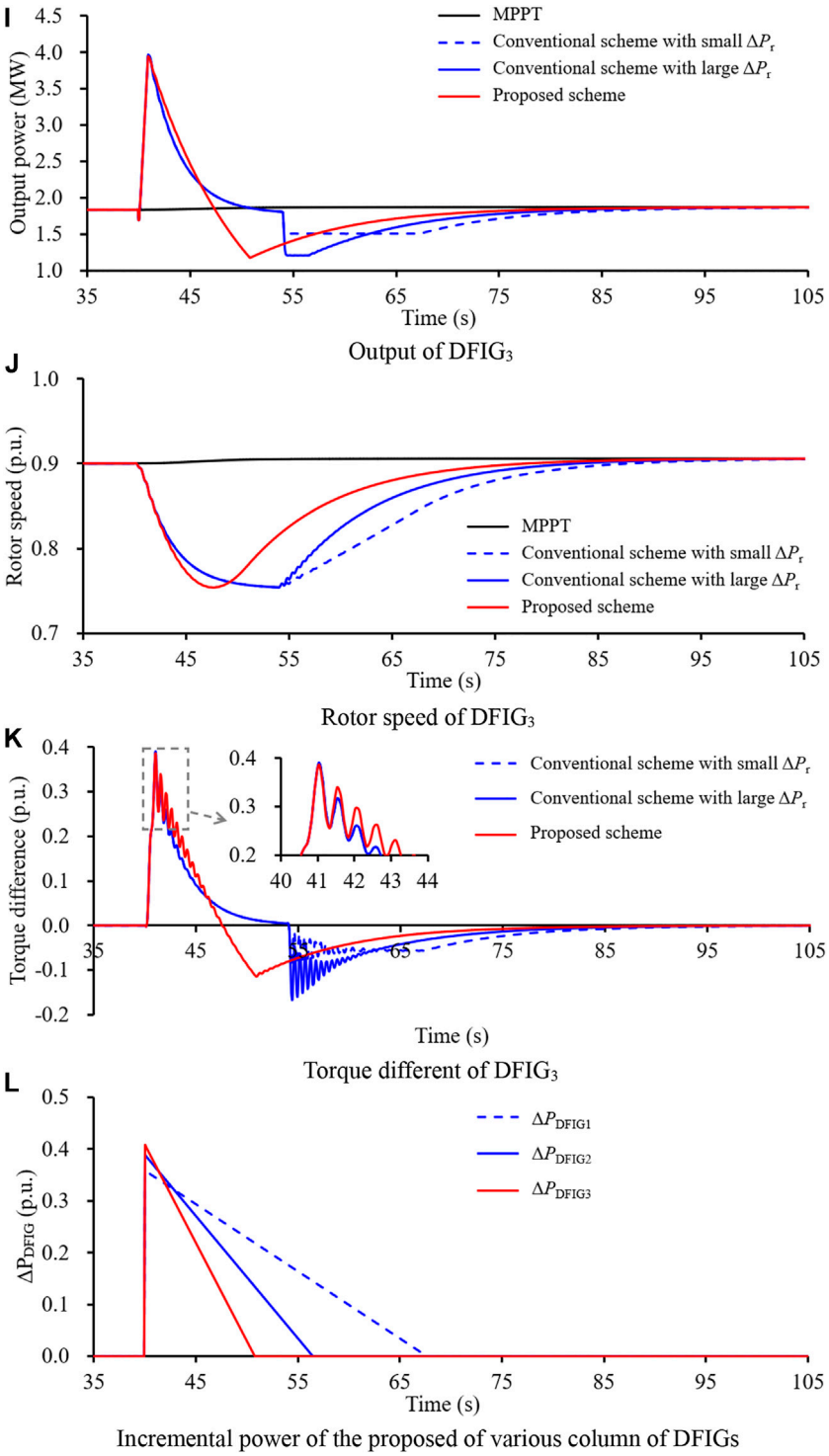

FIGURE 10
continued.

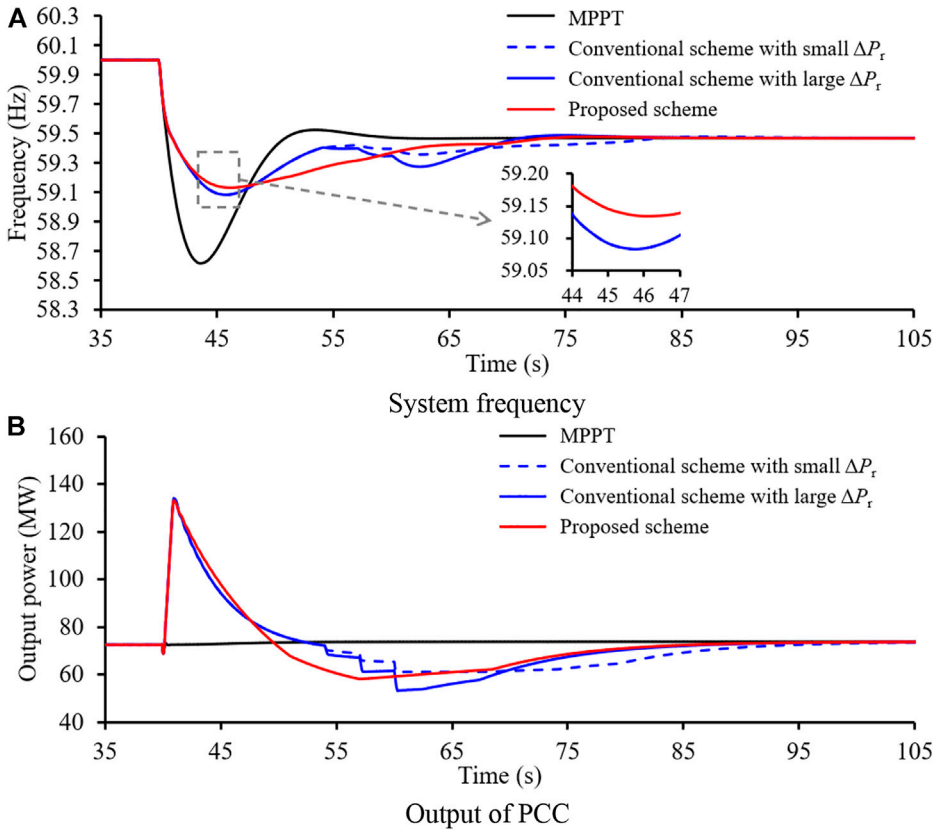

FIGURE 11
Results for case 2.

Conclusion

This study proposes a dynamic power-based temporary frequency support scheme for the wind power plant for minimizing the SFD while reducing the MFD. To this end, the reference of the output power increases to the torque limit. Afterward, the power reference smoothly decays with the dynamically decreasing incremental power and then automatically switches to the maximum power point tracking operation. Furthermore, to achieve realistic results, the wake effect is considered in this study.

The results indicate that the proposed stepwise IC strategy can improve the frequency nadir even though the same energy is released from the DFIGs as compared to the conventional stepwise IC schemes in the FSP. The depth of the SFD for the conventional stepwise IC scheme becomes notable and tends to be a lower value for a large wind generation-dominated power system; however, the proposed scheme can minimize the depth of the SFD and reduce mechanical stresses. Moreover, the performances with respect to reducing the MFD, reducing/removing the depth of the SFD, reducing mechanical stresses, and rapidly recovering the rotor speed are more notable in highly wind-penetrated power systems.

Data availability statement

The original contributions presented in the study are included in the article/Supplementary Materials; further inquiries can be directed to the corresponding author.

Author contributions

JY, DX, and JC designed the proposed strategy. All authors wrote and edited the manuscript.

Conflict of interest

The authors declare that the research was conducted in the absence of any commercial or financial relationships that could be construed as a potential conflict of interest.

Publisher's note

References

Boukhezzar, B., and Siguerdidjane, H. (2011). Nonlinear control of a variable speed wind turbine using a two mass model. *IEEE Trans. Energy Convers.* 26 (1), 149–162. doi:10.1109/tec.2010.2090155

Gevorgian, V., Zhang, Y., and Ela, E. (2015). Investigating the impacts of wind generation participation in interconnection frequency response. *IEEE Trans. Sustain. Energy* 6 (3), 1004–1012. doi:10.1109/tste.2014.2343836

Guo, X., Zhu, D., Zou, X., Yang, Y., Kang, Y., Tang, W., et al. (2022). Analysis and enhancement of active power transfer capability for DFIG-based WTs in very weak grid. *IEEE J. Emerg. Sel. Top. Power Electron.* 10, 3895–3906. doi:10.1109/JESTPE.2021.3089235

Hafiz, F., and Abdennour, A. (2015).Optimal use of kinetic energy for the inertial support from variable speed wind turbines, *Renew. Energy*, 80. 629. doi:10.1016/j.renene.2015.02.051

Hu, Y.-L., and Wu, Y.-K. (2019). Approximation to frequency control capability of a DFIG-based wind farm using a simple linear gain droop control. *IEEE Trans. Ind. Appl.* 55 (3), 2300–2309. doi:10.1109/tia.2018.2886993

Kang, M., Kim, K., Muljadi, E., Park, J. W., and Kang, Y. C. (2016). Frequency control support of a doubly-fed induction generator based on the torque limit. *IEEE Trans. Power Syst.* 31 (6), 4575–4583. doi:10.1109/tpwrs.2015.2514240

Kheshti, M., Ding, L., Nayeripour, M., Wang, X., and Terzijia, V. (2019). Active power support of wind turbines for grid frequency events using a reliable power reference scheme. *Renew. Energy* 139, 1241–1254. doi:10.1016/j.renene.2019.03.016

Koch, F., Gresch, M., Shewarega, F., Erlich, I., and Bachmann, U. (2005). "Consideration of wind farm wake effect in power system dynamic simulation," in Proc. Power Tech, 27-30 June 2005 (Russia: IEEE). doi:10.1109/PTC.2005.4524572

Lao, H., et al. .2020 Innovated inertia control of DFIG with dynamic rotor speed recovery. *CSEE J. Power & Energy Syst.*2096–0042 .doi:10.17775/CSEEJPES.2020.03180

Li, Y., Xu, Z., and Wong, K. P. (2017). Advanced control strategies of PMSG-based wind turbines for system inertia support. *IEEE Trans. Power Syst.* 32 (4), 3027–3037. doi:10.1109/tpwrs.2016.2616171

Morren, J., Pierik, J., and de Haan, S. W. H. (2006). Inertial response of variable speed wind turbines. *Electr. Power Syst. Res.* 76 (11), 980–987. doi:10.1016/j.epsr.2005.12.002

Peng, X., Yao, W., Yan, C., et al. (2020). Two-stage variable proportion coefficient based frequency support of grid connected DFIG-WTs. *IEEE Trans. Power Syst.*, 35, 962–974. doi:10.1109/TPWRS.2019.2943520

shi, Q., Li, F., and Cui, H. (2018). Analytical method to aggregate multi-machine SFR model with applications in power system dynamic studies. *IEEE Trans. Power Syst.* 33 (6), 6355–6367. doi:10.1109/tpwrs.2018.2824823

Technical standards GB (2018). *Wind turbines–Test procedure of gird adaptability*. Chinese: GB/T 36994.

Ullah, N. R., Thiringer, T., and Karlsson, D. (2008). Temporary primary frequency control support by variable speed wind turbines—potential and applications. *IEEE Trans. Power Syst.* 23 (2), 601–612. doi:10.1109/tpwrs.2008.920076

Vyver, J. V. d., Meersman, B., Vandevelde, L., and Vandoorn, T. L. (2016). Droop control as an alternative inertial response strategy for the synthetic inertia on wind turbines. *IEEE Trans. Power Syst.* 31 (2), 1129–1138. doi:10.1109/tpwrs.2015.2417758

Wang, J., Zhong, H., Yang, Z., Wang, M., Kammen, D. M., Zhu, L., et al. (2020). Exploring the trade-offs between electric heating policy and carbon mitigation in China. *Nat. Commun.* 11, 6054. doi:10.1038/s41467-020-19854-y

Wang, S., and Tomsovic, K. (2018). A novel active power control framework for wind turbine generators to improve frequency response. *IEEE Trans. Power Syst.* 33 (6), 6579–6589. doi:10.1109/tpwrs.2018.2829748

Wu, Y.-K., Yang, W. H., Hu, Y. L., et al. (2019). "Frequency regulation at a wind farm using a timing–varying inertia and droop controls," in ProceedingIEEE Trans. Ind. Appl., 07-10 May 2018.551 (Niagara Falls ON Canada: IEEE), 213–2224. doi:10.1109/ICPS.2018.8369978

Xiong, L., Liu, X., Liu, Y., and Zhuo, F.2020 Modeling and stability issues of voltage-source converter dominated power systems: A review. *CSEE J. Power Energy Syst.* (Early Access). doi:10.17775/CSEEJPES.2020.03590

Xiong, Y., Yao, W., Fen, J., Lin, S., Ai, X., Fang, J., et al. (2021). Two-level combined control scheme of VSC-mtdc integrated offshore wind farms for onshore system frequency support. *IEEE Trans. Power Syst.* 36 (1), 781–792. doi:10.1109/tpwrs.2020.2998579

Xu, G., and Xu, L. (2017). Improved use of WT kinetic energy for system frequency support. *IET Renew. Power Gener.* 11 (8), 1094–1100. doi:10.1049/iet-rpg.2016.0183

Yang, D., Jin, Z., Zheng, T., and Jin, E.2021 An adaptive droop control strategy with smooth rotor speed recovery capability for type III wind turbine generators. *Int. J. Electr. Power & Energy Syst.* 135, 107532. doi:10.1016/j.ijepes.2021.107532

Yang, D., Kim, J., Kang, Y. C., Muljadi, E., Zhang, N., Hong, J., et al. (2018). Temporary frequency support of a DFIG for high wind power penetration. *IEEE Trans. Power Syst.* 33 (3), 3428–3437. doi:10.1109/tpwrs.2018.2810841

Yang, D., Yan, G. -G., Zheng, T., Zhang, X., and Hua, L. (2022). Fast frequency response of a DFIG based on variable power point tracking control. *IEEE Trans. Ind. Appl.* 58 (4), 5127–5135. doi:10.1109/TIA.2022.3177590